Inorganic Chemistry

ARTICLE

pubs.acs.org/IC

Defect-Dicubane Ni_2Ln_2 (Ln = Dy, Tb) Single Molecule Magnets

Kartik Chandra Mondal,[†,‡] George E. Kostakis,[‡] Yanhua Lan,[†] Wolfgang Wernsdorfer,[§] Christopher E. Anson,[†] and Annie K. Powell*[,†,‡]

[†]Institute of Inorganic Chemistry, Karlsruhe Institute of Technology, Engesserstrasse 15, D-76131, Karlsruhe, Germany

[‡]Institute of Nanotechnology, Karlsruhe Institute of Technology, Hermann-von-Helmholtz Platz 1, 76344 Eggenstein-Leopoldshafen, Germany

[§]Institut Néel, CNRS and University J. Fourier, BP 166, 38042, Grenoble, Cedex 9, France

Supporting Information

ABSTRACT: Two pairs of Ni_2Dy_2 and Ni_2Tb_2 complexes, $[Ni_2Ln_2(L)_4(NO_3)_2(DMF)_2]$ {Ln = Dy (**1**), Tb (**2**)} and $[Ni_2Ln_2(L)_4(NO_3)_2(MeOH)_2]\cdot 3MeOH$ {Ln = Dy (**3**), Tb (**4**)} (H_2L is the Schiff base resulting from the condensation of *o*-vanillin and 2-aminophenol) possessing a defect-dicubane core topology were synthesized and characterized. All four complexes are ferromagnetically coupled, and the two Dy-analogues are found to be Single Molecule Magnets (SMMs) with energy barriers in the range 18−28 K. Compound **1** displays step-like hysteresis loops, confirming the SMM behavior. Although **1** and **3** show very similar structural topologies, the dynamic properties of **1** and **3** are different with blocking temperatures (3.2 and 4.2 K at a frequency of 1500 Hz) differing by 1 K. This appears to result from a change in orientation of the nitrate ligands on the Dy^{III} ions, induced by changes in ligands on Ni^{II}.

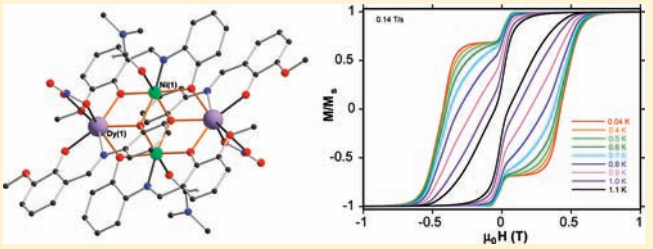

INTRODUCTION

Since the discovery of single molecule magnet (SMM) behavior in the $Mn_{12}Ac$ nanomagnet,[1] the search for new examples has been extensive in the light of possible applications for storing and processing magnetic information at a molecular level.[2] There are several synthetic strategies which can be applied to target new SMMs with the common aim of producing molecules with non-zero spin (S) and uniaxial (Ising) negative magnetic anisotropy (D).[2] Recently the strategy of combining 3d and 4f metal ions has gained favor since 3d ions can give rise to stronger magnetic coupling and/or magnetic anisotropy while 4f ions such as Dy^{III}, Tb^{III}, Ho^{III}, and so forth contribute large single-ion magnetic anisotropy.[3] The single-ion anisotropy of a metal ion depends mainly on its coordination geometry and ligand field[4] while the molecular anisotropy depends on several factors such as ligand field,[5a] relative orientation of the individual single-ion easy axes,[5b] magnetic coupling, and the structural topology of magnetic core.[5c,d]

On the other hand, the defect-dicubane (or "butterfly") core topology is one of the more familiar structural motifs in magnetochemistry, and coordination clusters of this type have been well studied and their behavior is often well understood. Defect-dicubane compounds such as $Mn^{III}_2Mn^{II}_2$,[6a] $Mn^{III}_2Ln^{III}_2$,[6b] $Fe^{III}_2Ln^{III}_2$[6c] have been found to exhibit SMM behavior with significant barriers to spin reorientation. Such behavior has also been seen in a variety of 3d-4f coordination clusters with different core topologies including examples with Cr-Ln,[7a] Mn-Ln,[7b,c] Fe-Ln,[7d] Co-Ln,[7e] Ni-Ln,[8] and Cu-Ln.[9]

As part of our efforts in this area we were interested to discover whether Ni-Ln combinations could be optimized to take advantage of the second order orbital angular momentum of Ni^{II} ions, which means that they also can provide large negative zero field splitting parameters. To date, among $Ni^{II}-Dy^{III}$ [10] compounds some of those ($NiDy_2$,[10e] NiDy[10e] and Ni_8Ln_8[10l]) show slow relaxation but without an observable maximum in χ'' vs T plots, while others ($NiDy_2$,[8a] Ni_2Dy,[8b] Ni_3Dy,[8e] and Ni_2Dy_2,[8f,g]) are found to be SMMs showing resolved maxima in χ'' vs T plots. Up to now, a tetranuclear linear $Ni^{II}_2Dy^{III}_2$[8f] compound has the highest energy barrier $\Delta \approx 17$ K among all Ni-Ln based SMMs.

With this in mind, and being motivated from our previous studies on magnetic coordination clusters,[6a,7a−7d,9] we chose to use the Schiff-base ligand ((*E*)-2-(2-hydroxy-3-methoxybenzylideneamino)phenol, (H_2L)[11] which has two types of pockets: Pocket-I, ONO-donating; Pocket-II, OO-donating (Scheme 1), one suitable to accommodate 3d and the other 4f ions. We report here the syntheses, characterization, and magnetic properties of four defect-dicubane coordination clusters formulated as $[Ni_2Ln_2(L)_4(NO_3)_2(DMF)_2]$ [Ln = Dy (**1**), Tb (**2**)] and $[Ni_2Ln_2(L)_4(NO_3)_2(MeOH)_2]\cdot 3MeOH$ [Ln = Dy (**3**), Tb (**4**)] and present a study of their magnetic relaxation dynamics showing the effect slight structural distortions may have on the magnetic characteristics.

EXPERIMENTAL SECTION

All chemicals and solvents used for synthesis were obtained from commercial sources and used as received without further purification. All reactions were carried out under aerobic conditions. The elemental

Received: July 19, 2011
Published: October 24, 2011

   dx.doi.org/10.1021/ic2015397 | *Inorg. Chem.* 2011, 50, 11604–11611

analyses (C, H, and N) were carried out at the Institute of Nanotechnology, Karlsruhe Institute of Technology, using an Elementar Vario EL analyzer. Fourier transform IR spectra (4000 to 400 cm^{-1}) were measured on a Perkin-Elmer Spectrum GX spectrometer with samples prepared as KBr discs. Powder X-ray diffraction was carried out on a STOE STADI-P diffractometer, using Cu−Kα radiation with λ = 1.5406 Å.

Synthetic Procedures. The Schiff-base ligand (H_2L) was synthesized using the reported general procedure,[11] condensing *o*-vanillin and 2-aminophenol in methanol.

Preparation of $[Ni_2Dy_2(L)_4(NO_3)_2(DMF)_2]$ (**1**). A mixture of $Dy(NO_3)_3\cdot 6H_2O$ (45 mg, 0.1 mmol), $Ni(NO_3)_2\cdot 6H_2O$ (29 mg, 0.1 mmol), and H_2L (48.6 mg, 0.2 mmol) was stirred in 10 mL of dimethylformamide (DMF) for 10−20 min in the presence of Et_3N (48 mg, 0.48 mmol). Red-brown block-shaped crystals of **1** were obtained from the resulting solution after two weeks in 90% yield. Anal. Calcd (%) for $C_{62}H_{58}O_{20}N_8Dy_2Ni_2$ (found): C 44.39 (44.45), N 6.68 (6.65), H 3.48 (3.50). IR (cm^{-1}): 3546 m, 3478s, 3414s, 3232w, 2924w, 1660s, 1605s, 1584 m, 1548 m, 1474s, 1455s, 1383s, 1398 m, 1384 m, 1297 m, 1228s, 1181s, 1108w, 1032w, 958w, 870w, 819 m, 744 m, 729 m, 685w, 637w, 584w, 517w.

Scheme 1. Structure of Ligand ((*E*)-2-(2-Hydroxy-3-methoxybenzylideneamino)phenol, (H_2L) with Two Types of Pocket (I and II)

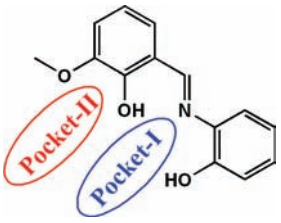

Preparation of $[Ni_2Tb_2(L)_4(NO_3)_2(DMF)_2]$ (**2**). The corresponding procedure using $Tb(NO_3)_3\cdot 6H_2O$ in place of $Dy(NO_3)_3\cdot 6H_2O$ was followed for the preparation of **2**, which was also obtained in 90% yield. Anal. Calcd (%) for $C_{62}H_{58}O_{20}N_8Tb_2Ni_2$ (found): C 44.58 (44.51), N 6.70 (6.67), H 3.50 (3.52). IR (cm^{-1}): 3546 m, 3478s, 3415s, 3232w, 2924w, 1661s, 1605s, 1584 m, 1548 m, 1476s, 1455s, 1382s, 1398 m, 1384 m, 1297 m, 1228s, 1182s, 1108w, 1032w, 958w, 870w, 819 m, 744 m, 730 m, 685w, 637w, 585w, 518w.

Preparation of $[Ni_2Dy_2(L)_4(NO_3)_2(MeOH)_2]\cdot 3MeOH$ (**3**). A mixture of $Dy(NO_3)_3\cdot 6H_2O$ (45 mg, 0.1 mmol), $Ni(NO_3)_2\cdot 6H_2O$ (29 mg, 0.1 mmol), and H_2L (48.6 mg, 0.2 mmol) was stirred in 10 mL of MeOH for 5−10 min in the presence of Et_3N (48 mg, 0.48 mmol). The resulting yellow-green solution was left undisturbed and small hexagonal greenish-yellow crystals of **3** formed after 12 h in 90% yield. Anal. Calcd (%) for $C_{61}H_{64}N_6O_{23}Dy_2Ni_2$ (found): C 43.31 (43.23), N 4.97 (5.02), H 3.81 (3.75). IR (KBr, cm^{-1}): 3414b, 3057w, 2942w, 2835w, 1606s, 1586s, 1546 m, 1517s, 1481s, 1459s, 1439s, 1386s, 1331 m, 1290 m, 1255 m, 1225s, 1182w, 1108w, 1075w, 1019w, 966 m, 822w, 737s, 642w, 588w, 520w.

Preparation of $[Ni_2Tb_2(L)_4(NO_3)_2(MeOH)_2]\cdot 3MeOH$ (**4**). The corresponding procedure using $Tb(NO_3)_3\cdot 6H_2O$ in place of $Dy(NO_3)_3\cdot 6H_2O$ was followed for the preparation of **2**, which was also obtained in 91% yield. Anal. Calcd (%) for $C_{61}H_{64}N_6O_{23}Tb_2Ni_2$ (found): C 43.50 (43.45), N 4.99 (5.15), H 3.83 (3.55). IR (KBr, cm^{-1}): 3414b, 3055w, 2942w, 2835w, 1606s, 1585s, 1546 m, 1517s, 1482s, 1459s, 1439s, 1386s, 1331 m, 1291 m, 1255 m, 1225s, 1182w, 1108w, 1075w, 1019w, 966 m, 822w, 734s, 644w, 589w, 520w.

Magnetic Measurements. The magnetic susceptibility measurements were obtained using a Quantum Design SQUID magnetometer MPMS-

Table 1. Crystallographic Data and Refinement Parameters for 1 and 4, with Unit Cells for 2 and 3

	1	2	3	4
formula	$C_{62}H_{58}Dy_2N_8Ni_2O_{20}$	$C_{62}H_{58}Tb_2N_8Ni_2O_{20}$	$C_{61}H_{64}N_6Ni_2O_{23}Dy_2$	$C_{61}H_{64}N_6Ni_2O_{23}Tb_2$
M_r (g/mol)	1677.58			1684.44
cryst size[mm]	0.39 × 0.34 × 0.16			0.14 × 0.12 × 0.10
color	green-yellow	green-yellow	green	green
cryst syst	monoclinic	monoclinic	monoclinic	monoclinic
space group	$P2_1/n$	$P2_1/n$	$P2_1/c$	$P2_1/c$
a [Å]	13.2070(11)	13.236(2)	11.973(2)	12.0955(10)
b [Å]	12.9862(8)	12.875(2)	24.147(4)	24.2560(11)
c [Å]	18.1372(16)	18.254(3)	11.166(2)	11.2336(8)
β [deg]	90.210(7)	90.280(13)	108.507(3)	107.996(6)
V [$Å^3$]	3110.7(4)	3110.5(8)	3061.3(16)	3134.6(4)
T [K]	150(2)	180(2)	100(2)	180(2)
Z	2	2	2	2
ρ_{calcd} [g cm^{-3}]	1.791			1.785
μ(Mo−Kα) [mm^{-1}]	3.054			2.906
F(000)	1668			1684
data collected	26103			18980
unique data	7450			6637
R_{int}	0.0479			0.0535
data with $I > 2\sigma(I)$	5563			4361
parameters/restraints	428/0			420/17
S on F^2 (all data)	0.978			1.020
wR_2 (all data)	0.1281			0.1582
R_1 [$I > 2\sigma(I)$]	0.0516			0.0632
max. difference peak/hole [e $Å^{-3}$]	1.36/−3.04			3.22/−1.30

dx.doi.org/10.1021/ic2015397 |*Inorg. Chem.* 2011, 50, 11604–11611

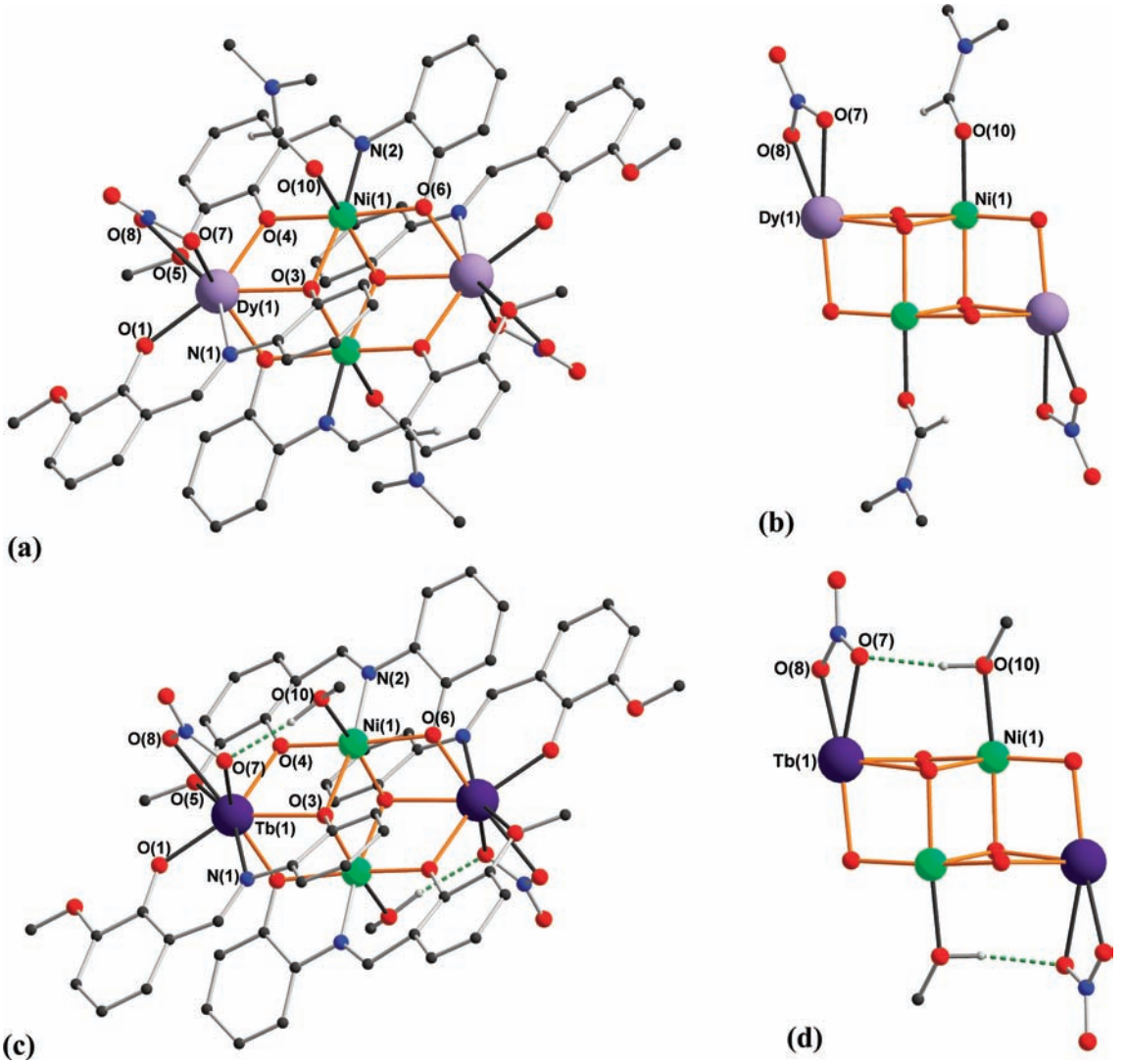

Figure 1. Molecular structures of the coordination clusters in compounds **1** (a) and **4** (c), and the geometries of the DMF, MeOH and nitrate ligands relative to the cluster cores (b and d). Organic H-atoms are omitted for clarity; Dy violet, Tb dark purple, O red, N blue, C black, H white.

Scheme 2. Observed Bridging Modes of the Dianionic Ligand (L^{2-}) in Complexes 1−4

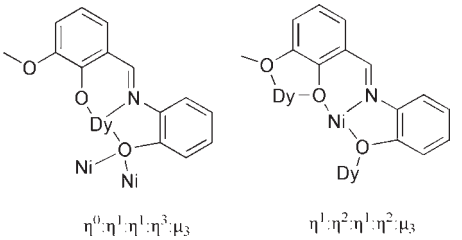

$\eta^0{:}\eta^1{:}\eta^1{:}\eta^3{:}\mu_3$ $\eta^1{:}\eta^2{:}\eta^1{:}\eta^2{:}\mu_3$

XL in the temperature range 1.8−300 K. Measurements were performed on polycrystalline samples of 10.6, 5.0, 8.2, and 10.5 mg for **1**−**4**, respectively. Alternating current (ac) susceptibility measurements were performed with an oscillating field of 3 Oe and ac frequencies ranging from 1 to 1500 Hz. *M* versus *H* measurements were performed at 100 K to check for the presence of ferromagnetic impurities; none were found. The magnetic data were corrected for the sample holder and the diamagnetic contribution. Magnetization measurements on oriented single crystals were carried out using an array of micro-SQUIDs, working in the temperature range of 0.04 to about 7 K and in fields of up to 0.8 T with sweeping rates as high as 0.28 T s^{-1}, and exhibiting field stability of better than 1 μT. The time resolution is approximately 1 ms, and the field can be applied in any direction of the micro-SQUID plane with precision better than 0.1° by separately driving three orthogonal coils.[12] To ensure good thermalization, a single crystal was fixed with eicosane.

X-ray Crystallography. Data for **1**−**4** were collected at 150 or 180 K on Stoe IPDS II area detector diffractometers using graphite-monochromated Mo−Kα radiation. Semiempirical absorption corrections were applied using XPREP within SHELXTL.[13] The structures were solved using direct methods, followed by full-matrix least-squares refinement against F^2 (all data) using SHELXTL.[13] All non-hydrogen atoms were refined anisotropically, with the exception of five carbon atoms in a disordered aromatic ring and the atoms of the disordered methanol solvate molecules in **4**, which were refined isotropically with half-occupancy. Organic hydrogen atoms were placed in calculated positions; the coordinates of the O−H hydrogen atom in 4 were refined. Crystallographic and structure refinement data are summarized in Table 1. Crystallographic data (excluding structure factors) for the structures in this paper have been deposited with the Cambridge Crystallographic

dx.doi.org/10.1021/ic2015397 |*Inorg. Chem.* 2011, 50, 11604–11611

Table 2. Direct Current Magnetic Data for Compounds 1−4

compound	ground state of Ln^{III} ion	χT expected for non-interacting ions/measured at 300 K/measured at 1.8 K per complex (cm^3 K mol^{-1})	magnetization at 2 K and 7 T (μ_B)
Ni_2Dy_2(DMF), **1**	$^6H_{15/2}$	30.34/30.61/58.97	14.26
Ni_2Tb_2(DMF), **2**	$^7H_6$	25.64/26.77/35.35	14.35
Ni_2Dy_2(MeOH), **3**	$^6H_{15/2}$	30.34/31.11/60.28	14.70
Ni_2Tb_2(MeOH), **4**	$^7H_6$	25.64/26.64/41.79	13.79

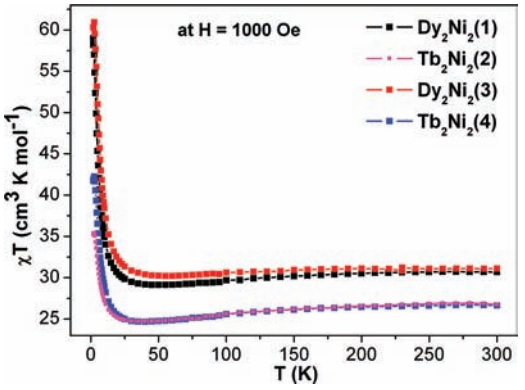

Figure 2. Plots of χT vs T for **1**−**4** under applied dc magnetic field of 1000 Oe.

Data Centre as supplementary publication nos. CCDC 833229 and 833230. Copies of the data can be obtained, free of charge, on application to CCDC, 12 Union Road, Cambridge CB2 1EZ, U.K: http://www.ccdc.cam.ac.uk/cgi-bin/catreq.cgi, e-mail: data_request@ccdc.cam.ac.uk, or fax: +44 1223 336033.

RESULTS AND DISCUSSION

Synthesis. All four compounds were obtained in high yield from the reaction of $Ln(NO_3)_3 \cdot 6H_2O$, $Ni(NO_3)_2 \cdot 6H_2O$, and H_2L in the presence of Et_3N as base in the molar ratio of 1:1:2:5, either in DMF (**1**−**2**) or MeOH (**3**−**4**) as solvent. Changes to the molar ratio by decreasing the amount of the ligand and increasing the amount of metal salt result in different products, which will be described elsewhere.

Description of the Structures. A combination of single-crystal and powder diffraction measurements established that all compounds are isostructural. Compounds **2** and **3** consistently gave crystals of rather poor quality, such that their structures could not be refined to an adequate standard. However, their unit cells and powder diffraction (Tables 1, Supporting Information, Figure S1) show that compounds **1** and **2**, and **3** and **4**, forming isomorphous pairs, respectively, and elemental analyses confirmed that **1** and **2**, and **3** and **4**, have the same formulation. The only significant difference in the molecular structures involves the replacement of the DMF ligand on each Ni^{II} ion in **1** and **2** by MeOH ligands in **3** and **4**.

Here we will describe the structure of **1** in detail; it crystallizes in the monoclinic space group $P2_1/n$ with $Z = 2$ such that the molecule has centrosymmetric site symmetry in the crystal (Figure 1a). The Ni^{II} ion has adopted a slightly distorted octahedral geometry with an O_5N donor set, while the Dy^{III} ion has a distorted square antiprismatic geometry with an O_7N donor set. The Ni^{II} ion is chelated by the ONO atoms of Pocket-I (Scheme 1) of one of the two independent ligands in the structure, with these two deprotonated phenoxo oxygens each forming μ_2-bridges from the chelated Ni^{II} to different Dy^{III} ions, one of which is chelated by Pocket-II of this ligand. The other independent ligand coordinates rather differently, with Pocket-I rather unexpectedly chelating a Dy^{III} ion. The vanillin-derived phenoxo oxygen, although deprotonated, does not coordinate to other metal centers, and Pocket-II of the ligand is thus empty. The aminophenol oxygen, by contrast, forms a μ_3-bridge over a Ni_2Dy triangle. The coordination modes of the two ligands are shown in Scheme 2. Two such triply bridging oxygens coordinate to each Ni^{II} ion, with a DMF ligand coordinating through oxygen completing the O_5N environment of each Ni center. Each Dy^{III} ion is ligated by Pocket-I (ONO) of one ligand type, and Pocket-II (OO) of the other independent ligand from opposite directions, filling five coordination sites in a distorted pentagonal-planar geometry. The sixth coordination site is occupied by a μ_2-phenoxo oxygen from the aminophenol part of a third Schiff-base ligand, and the seventh and eighth sites are filled by two oxygen atoms of a chelating nitrate ligand. The DMF ligands each form weak hydrogen bonds; the aldehydic C−H interacts with the oxygen atom O(7) of the nitrate ligand, with a C···O distance of 3.354 Å.

The core of compound **1** can be described in terms of the well-known defect-dicubane or butterfly topology with two Ni^{II} ions in the *body* positions and each Dy^{III} ion in the *wing* positions.-(Supporting Information, Figure S2). The four Ni−Dy edges are each bridged by μ_2-phenoxo oxygens from two symmetry-related ligands, while the two other ligands form μ_3-bridges over the two Ni_2Dy triangles with O(3) displaced by 1.052 Å out of the Ni_2Dy plane, on opposite sides of the strictly planar Ni_2Dy_2 core.

The molecular structure of **4**, which crystallizes in the space group $P2_1/n$ with $Z = 2$, and thus also has crystallographically imposed inversion symmetry, has the same connectivity as for **1**, the only difference being the replacement of the DMF ligands in **1** by methanol ligands in **4** (Figure 1c). Any differences between corresponding bond lengths and angles in the metal coordination spheres of **1** and **4** are in general small, and are mostly not statistically significant, even though the lanthanide ions do not have the same ionic radii. However, replacing the terminal DMF ligand on Ni(1) in **1** by a methanol in **4** does have a very significant effect on the nitrate ligands. In **4**, the methanol can hydrogen bond to oxygen O(7) of the nitrate, with O(10)···O(7) 2.898 Å. By contrast, the DMF ligand in **1** is oriented approximately coparallel with the nitrate ligand, so that any interaction is $\pi-\pi$ in nature, rather than a C−H··O hydrogen bond; O(10)···O(7) is now 3.410 Å.

Although, as already stated, there are no obvious changes in the Ln−O or Ni−O bond lengths, the effects of the ligand substitution become very clear if one now considers the orientation of the nitrate ligands relative to their respective cluster cores. In **1**, the Ni(1)···Dy(1)−O(7) angle is 88.6°, but in **4**, with the stronger and shorter hydrogen bond, the Ni(1)···Tb(1)−O(7)

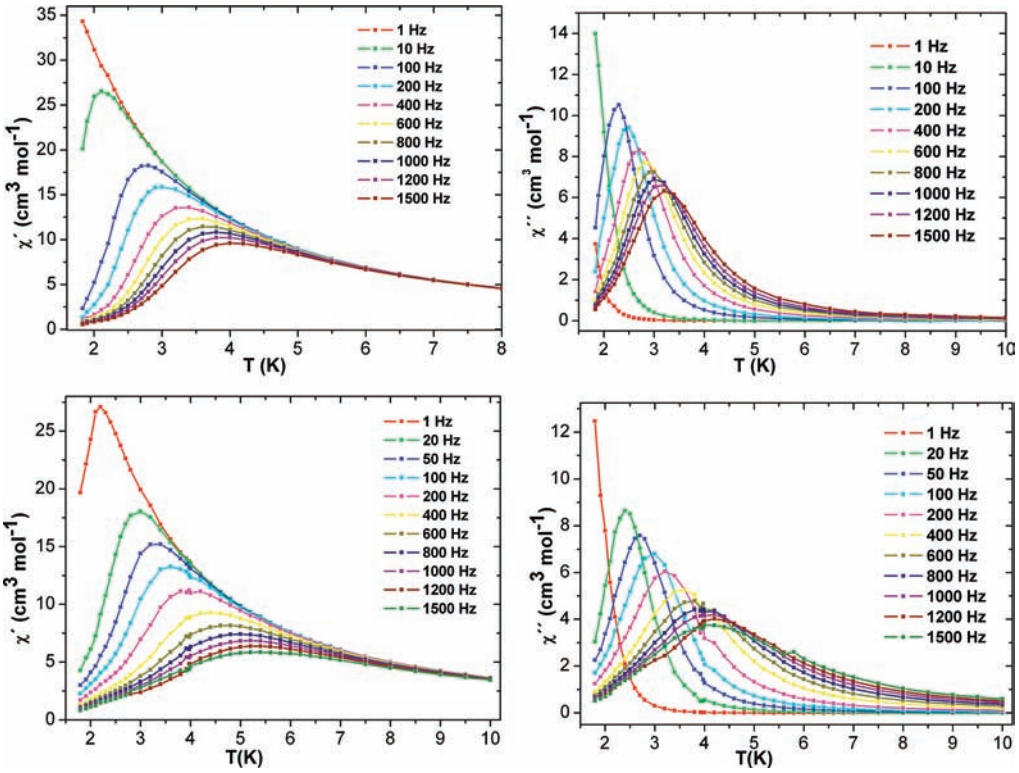

Figure 3. Plots of in-phase (χ') vs T (left) and out-of-phase (χ'') vs T (right) of **1** (top) and **3** (bottom).

Table 3. Comparison of the ac Magnetic Data for Compounds 1−4[a]

compounds	detectable out-of-phase signal	T_b (at 1500 Hz)	Δ (K) and τ_0 (s) under H_{dc} = 0	Δ (K) and τ_0 (s) under H_{dc} = 4000 Oe
Ni_2Dy_2(DMF), **1**	yes	3.2 K	18.5; 5.4×10^{-7}	effective QT but without further measurements
Ni_2Tb_2(DMF), **2**	no	well below 1.8 K		
Ni_2Dy_2(MeOH), **3**	yes	4.2 K	21.3; 1.5×10^{-6}	effective QT, 28.5; 2.8×10^{-6}
Ni_2Tb_2(MeOH), **4**	yes	below 1.8 K		no obvious QT

[a] T_b is the blocking temperature; Δ is the energy gap to the reversal of magnetization; τ_0 is the relaxation time. See the text for further details.

angle has been reduced to 79.8° so that in comparison to **1**, the nitrate ligand in **4** has been tipped toward Ni(1) by about 10°. The corresponding angles involving the other chelating oxygen of the nitrate, O(8), are 105.2° and 98.7° for **1** and **4**, respectively; the smaller difference implies that as well as being tipped toward Ni(1), the nitrate is also slightly twisted between the two compounds (Figure 1b, 1d). The change in Ln(1)···Ni(1)−O(10) angles is smaller: 89.5° for the DMF ligand in **1**, reducing to 85.1° for the methanol in **4**. It seems somewhat paradoxical that a ligand substitution on the Ni^{II} centers has, in fact, a greater effect on the geometries around the Dy^{III} ions than on those about the Ni^{II} ions themselves. Such differences will be seen to have significant effects on the magnetic behavior of the two compounds.

Magnetic Studies. The temperature dependence of the magnetic susceptibilities of complexes **1**−**4** were each measured on powdered samples over the temperature range 1.8−300 K under an applied direct current (dc) magnetic field of 1000 Oe. The χT values of **1**−**4** at room temperature are in good agreement (see Table 2) with the theoretically expected χT values for the noninteracting ions.[14] The χT products of **1**−**4** all decrease slightly with decreasing temperature, reaching minimum values of 29.12 (**1**), 24.72 (**2**), 39.20 (**3**), and 24.67 cm^3 K mol^{-1} (**4**) at 50 K (**1**,**3**) and 40 K (**2**,**4**). In each case, on further decreasing the temperature, this is followed by a sharp rise to 58.97 (**1**), 35.35 (**2**), 60.28 (**3**), and 41.79 cm^3 K mol^{-1} (**4**), respectively, at 1.8 K (Figure 2). The shape of the χT vs T plots indicates intramolecular ferromagnetic interactions between the paramagnetic centers within the defect-dicubane units. The slight decrease in χT on decreasing the temperature from 300 to 50 K can be ascribed to the thermal depopulation of Stark sublevels of the Dy^{III} or Tb^{III} ions.[3b,7−10]

The field dependence of magnetization for **1**−**4** each shows an initial rapid increase up to a field of 10 kOe, followed by almost linear increase with field, finally reaching values of 14.26 (**1**), 14.35 (**2**), 14.70 (**3**), and 13.79 μ_B (**4**) at 70 kOe and 2 K, but without a true saturation (Supporting Information, Figures S3−S4). The sharp increase of M values at lower dc field (Supporting Information, Figures S3−S4) also indicates the presence of intramolecular ferromagnetic interactions. Furthermore, the M vs H/T plots of **1**−**4** at different temperatures are not superposed, indicating the presence of low lying energy states and/or anisotropy in the system.[3b,7−10]

dx.doi.org/10.1021/ic2015397 |*Inorg. Chem.* 2011, 50, 11604–11611

Variable-temperature ac susceptibility measurements as a function of both temperature and frequency were carried out under zero dc fields. A strong frequency-dependence of the in-phase (χ') and out-of-phase (χ'') signals was observed for both Dy-containing complexes **1** and **3** (Figure 3 and Supporting Information, Figure S5), but only a weak frequency–dependence of the out-of-phase signals below 6 K (without a maximum in plots of χ' and χ'' vs T above 1.8 K) for the Ni^{II}_2-Tb^{III}_2 complex **4**. (Supporting Information, Figure S6) No out-of-phase signals were observed for **2** above 1.8 K. The blocking temperatures (T_b, maximum of χ'' vs T plot) at 1500 Hz for **1** and **3** could be observed at 3.2 and 4.2 K, respectively, but those for the Tb-containing complexes **2** and **4** lie well below 1.8 K (Table 3).

Frequency-dependent ac measurements were made at 1.8 K under different applied magnetic fields to investigate the existence of any Quantum tunneling of Magnetization (QTM) effects in these compounds. Through QTM, the magnetic relaxation of an SMM from one magnetic state to that of opposite spin can be faster than predicted from the barrier height because of tunneling through the relaxation energy barrier, but this can be suppressed (partially or totally) by application of a dc field, which lifts the degeneracy of corresponding spin levels on either side of the barrier. Complexes **1**–**4** were therefore probed further by ac measurements made under a range of small external fields. The Ni_2Dy_2 complexes **1** and **3** show efficient QTM effects (Supporting Information, Figure S7) under fields below 4000 Oe, but such effects are not obviously observed in the Ni_2Tb_2 complex **4** (Supporting Information, Figure S9). The ac (χ' and χ'') susceptibilities of **3** were recorded under an applied dc magnetic field of 4000 Oe to suppress QTM pathways, and its blocking temperature was then found to increase from 4.2 to 5.5 K (Supporting Information, Figure S8).

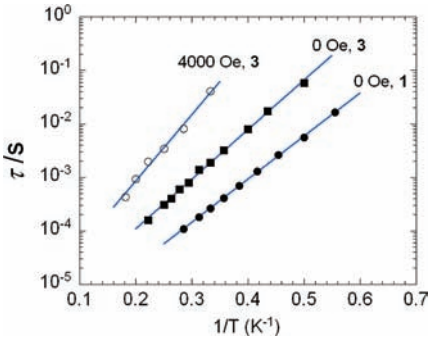

Figure 4. Arrhenius semilog plots of the relaxation time, τ, vs $1/T$ of complexes **1** and **3** from ac susceptibility measurements both under zero and an applied dc field of 4000 Oe. The solid lines correspond to a linear fit in the thermally activated range of temperatures.

Linear Arrhenius fitting (τ vs $1/T$) of the data for **1** and **3** measured under zero applied magnetic field (Figure 4) results in energy barriers (Δ) of 18.5 (**1**) and 21.3 K (**3**) with relaxation times $\tau_0 = 5.4 \times 10^{-7}$ ($R = 0.999$, **1**) and 1.5×10^{-6} s ($R = 0.998$, **3**). The energy barrier of **3** was found to increase to 28.5 K with $\tau_0 = 2.8 \times 10^{-6}$ s on fitting the data measured under a dc field of 4000 Oe, indicating that the application of an external field has indeed suppressed QTM, confirming the presence of such effects in compound **3**.

The Cole–Cole diagram (χ'' vs χ' at different temperatures) can be used to study the distribution of the relaxation process, which is frequently characterized and discussed for SMMs or SCMs. The data of **1** and **3** plotted as Cole–Cole diagrams are shown in Figure 5. The shape of the Cole–Cole plot of **1** is relatively symmetrical and can be fitted to the generalized Debye model[15] with a parameter α ranging from 0.14 to 0.10 (Supporting Information, Table S3). The small α value suggests that there is only one relaxation process present in **1**. However, the Cole–Cole plot of **3** is rather unsymmetrical below 3.2 K. A good fit to the generalized Debye model could only be obtained above 3.4 K giving an α value of 0.09–0.16. These results indicate that the crossover from the thermally activated relaxation process to a quantum regime might start to occur in this system below 3.2 K.

To confirm the SMM behavior, micro-SQUID measurements[12] were performed on a single crystal of **1**. Hysteresis loops are clearly detected at low temperatures below 1.1 K (Figure 6). A coercive field of 0.5 T is observed at a temperature of 0.04 K and a field sweep rate of 0.14 T/s, and the coercive fields increase with increasing field sweeping rate from 0.001 to 0.280 T/s. The width of the loops is strongly temperature and sweep rate dependent, as would be expected for the superparamagnetic-like behavior. The step-like features of the hysteresis loops confirm the presence of resonant quantum tunneling effects in this system, as already demonstrated by the ac susceptibility measurements. The step-like feature becomes more prominent below 1.0 K. The sweep rate dependent hysteresis loops at a constant temperature of 0.04 K (Figure 6, right) reveal that there are two steps: one at close to zero magnetic field and another between 0.4 to 0.5 T. The large relaxation step at zero magnetic field is probably related to fast quantum tunneling of the

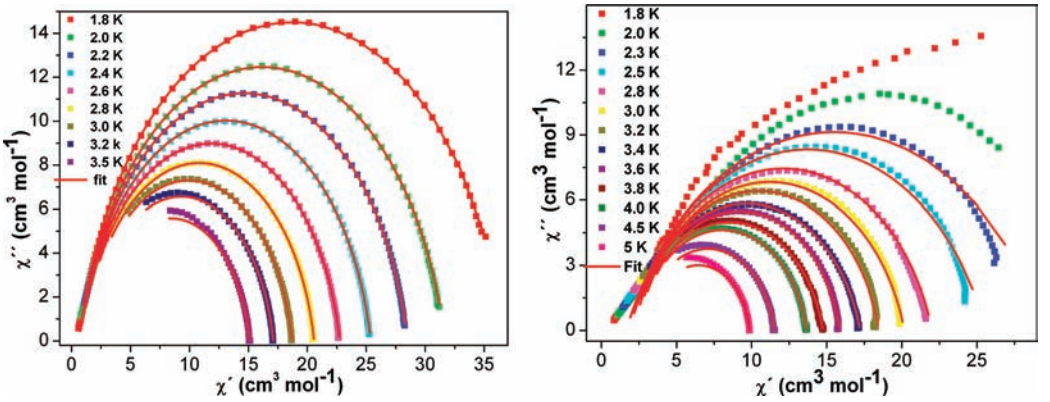

Figure 5. Cole–Cole plots of **1** (left) and **3** (right) under zero applied dc field. The solid lines correspond to the fit to the generalized Debye model.

dx.doi.org/10.1021/ic2015397 |*Inorg. Chem.* 2011, 50, 11604–11611

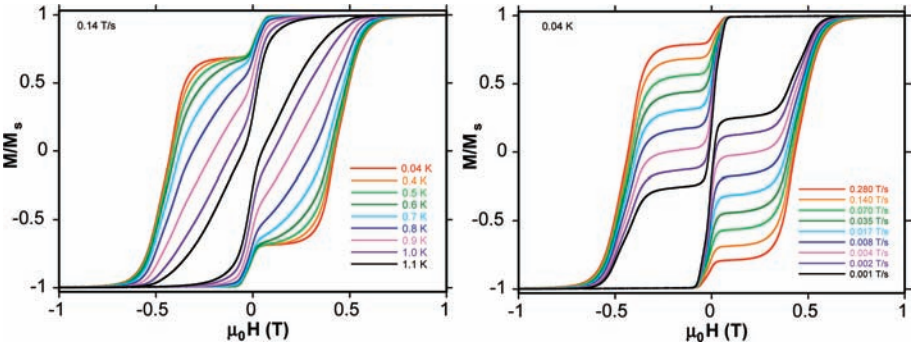

Figure 6. Normalized magnetization (M being normalized at the saturated magnetization M_S) of **1** vs applied field (μ_oH). The loops are shown at different temperatures with a sweep rate of 0.14 T/s (left) and at different sweep rates at 0.04 K (right).

magnetization (QTM) through the ground Kramer states, which has been commonly observed in many SMMs containing Dy^{III} ions.[3] We have also tried to carry out the dc magnetization decay measurements (Supporting Information, Figure S10) to assess the relaxation time; however, the tunneling is so strong that the dc data are not reliable (Supporting Information, Figure S11). All these results show that complex **1** is a SMM, with the highest energy barrier of any Ni-Ln SMM so far reported.

CONCLUSION

We have utilized a Schiff base pocket ligand to synthesize heterometallic polynuclear 3d/4f coordination clusters. The four compounds with defect-dicubane Ni_2Dy_2 and Ni_2Tb_2 topologies reported here represent the first 3d-4f complexes with this ligand. The dc magnetic measurements show that all four complexes are ferromagnetically coupled. Alternating current magnetic studies show that the Ni_2Dy_2 compounds **1** and **3** are SMMs with effective energy barriers (Δ) of 18.5 (**1**) and 21.3 K (**3**) under zero applied magnetic field with respective relaxation times $\tau_0 = 5.4 \times 10^{-7}$ and 1.5×10^{-6} s. The energy barrier for **3** was found to increase to 28.5 K with $\tau_0 = 2.8 \times 10^{-6}$ s under applied dc magnetic field of 4000 Oe. The Ni_2Tb_2 compound **4** also exhibits detectable out-of-phase signals but without observable maxima, suggesting that **4** might be also a SMM but with a blocking temperature below 1.8 K. Fittings to the Cole−Cole plots for **1** and **3** using a generalized Debye model produce small values for the α parameter, indicating one single thermal relaxation process is dominant in these systems. The SMM behavior in **1** was confirmed by temperature and sweep rate dependent step-like hysteresis loops. Compounds **1** and **3** possess the highest effective energy barriers among all the Ni-Ln based SMMs so far reported.

Comparing the corresponding Ni_2Dy_2 and Ni_2Tb_2 systems (**1** with **2**; **3** with **4**), it is clear that the anisotropy of the Ln^{III} ions (Dy^{III} versus Tb^{III}) is the more important parameter determining SMM behavior than the total spin of the system (which is higher for the Tb^{III}-containing clusters), resulting in the better dynamic properties in the Dy^{III}-containing systems. If one now compares the dynamic behaviors of the two Ni_2Dy_2, and the two Ni_2Tb_2, compounds, both pairs show a similar trend, with the two complexes with methanol ligands on the Ni^{II} ions both showing a higher energy barrier than their corresponding DMF analogues. Although intermolecular hydrogen bonding can in principle suppress QTM at zero field in lanthanide-containing systems,[3] any such interactions via the disordered lattice methanols in compounds **3** and **4** will be very weak, and can be disregarded here. As discussed earlier in the context of the structures, this ligand substitution on Ni^{II} in fact has a larger effect on the geometries of the ligand shell about the lanthanides, and this has clearly had a significant effect on the orientation, and presumably the magnitude, of the lanthanide Single-Ion Anisotropy tensors. It can be concluded that, when comparing the structures of related lanthanide-based SMMs to rationalize differences in dynamic magnetic behavior, it can be more important to consider changes in ligand orientation relative to the cluster core as a frame of reference, rather than simply comparing lists of bond lengths and angles.

ASSOCIATED CONTENT

Supporting Information. Additional information in the form of Figures S1−S11, Table S1−S4, synthetic part and crystallographic data in CIF format. This material is available free of charge via the Internet at http://pubs.acs.org.

AUTHOR INFORMATION

Corresponding Author
*E-mail: annie.powell@kit.edu.

ACKNOWLEDGMENT

The authors gratefully acknowledge financial from the DFG Center for Functional Nanostructures.

REFERENCES

(1) (a) Caneschi, A.; Gatteschi, D.; Sessoli, R. *J. Am. Chem. Soc.* **1991**, *113*, 5873. (b) Thomas, L.; Lionti, F.; Ballou, R.; Gatteschi, D.; Sessoli, R.; Barbara, B. *Nature* **1996**, *383*, 145.

(2) Caneschi, A.; Gatteschi, D.; Sessoli, R. *Angew. Chem., Int. Ed.* **2003**, *42*, 268.

(3) (a) Benelli, C.; Gatteschi, D. *Chem. Rev.* **2002**, *102*, 2369. (b) Sessoli, R.; Powell, A. K. *Coord. Chem. Rev.* **2009**, *253*, 2328. (c) Sorace, L.; Benelli, C.; Gatteschi, D. *Chem. Soc. Rev.* **2011**, *40*, 3092–3104.

(4) Freedman, D. E.; Harman, W. H.; Harris, T. D.; Long, G. J.; Chang, C. J.; Long, J. R. *J. Am. Chem. Soc.* **2010**, *132*, 1224.

(5) (a) Ishikawa, N. *Polyhedron* **2007**, *26*, 2147. (b) Liu, J.-L.; Guo, F.-S.; Meng, Z. S.; Zheng, Y.-Z.; Leng, J.-D.; Tong, M. L.; Ungur, L.; Chibotaru, L.; Heroux, K. J.; Hendrickson, D. N. *Chem. Sci.* **2011**, *2*, 1268. (c) Chakov, N. E.; Soler, M.; Wernsdorfer, W.; Abboud, K. A.; Christou, G. *Inorg. Chem.* **2005**, *44*, 5304. (d) King, P.; Wernsdorfer, W.; Abboud, K. A.; Christou, G. *Inorg. Chem.* **2005**, *44*, 8659.

(6) (a) Ako, A. M.; Mereacre, V.; Hewitt, I. J.; Clérac, R.; Lecren, L.; Anson, C. E.; Powell, A. K. *J. Mater. Chem.* **2006**, *16*, 2579. (b) Mishra,

A.; Wernsdorfer, W.; Parsons, S.; Christou, G.; Brechin, E. K. *Chem. Commun.* **2005**, 2086. (c) Murugesu, M.; Mishra, A.; Wernsdorfer, W.; Abboud, K. A.; Christou., G. *Polyhedron* **2006**, *25*, 613.

(7) (a) Rinck, J.; Novitchi, G.; Heuvel, W. V. d.; Ungur, L.; Lan, Y.; Wernsdorfer, W.; Anson, C. E.; Chibotaru, L. F.; Powell, A. K. *Angew. Chem., Int. Ed.* **2010**, *49*, 7583. (b) Mereacre, V.; Ako, A: M.; Clérac, R.; Wernsdorfer, W.; Hewitt, I. J.; Anson, C. E.; Powell, A. K. *Chem.—Eur. J.* **2008**, *14*, 3577. (c) Mereacre, V.; Lan, Y.; Clerac, R.; Ako, A. M.; Hewitt, I. J.; Wernsdorfer, W.; Buth, G.; Anson, C. E.; Powell, A. K. *Inorg. Chem.* **2010**, *49*, 5293. (d) Schray, D.; Abbas, G.; Lan, Y.; Mereacre, V.; Sundt, A.; Dreiser, J.; Waldmann, O.; Kostakis, G. E.; Anson, C. E.; Powell, A. K. *Angew. Chem., Int. Ed.* **2010**, *49*, 5185. (e) Chandrasekhar, V.; Pandian, B. M.; Azhakar, R.; Vittal, J. J.; Clérac, R. *Inorg. Chem.* **2007**, *46*, 5140.

(8) (a) Pointillart, E.; Bernot, K.; Sessoli, R.; Gatteschi, D. *Chem.—Eur. J.* **2007**, *13*, 1602. (b) Chandrasekhar, V.; Pandian, B. M.; Boomishankar, R.; Steiner, A.; Vittal, J. J.; Houri, A.; Clérac, R. *Inorg. Chem.* **2008**, *47*, 4918. (c) Sutter, J.-P.; Dhers, S.; Rajamani, R.; Ramasesha, S.; Costes, J.-P.; Duhayon, C.; Vendier, L. *Inorg. Chem.* **2009**, *48*, 5820. (d) Efthymiou, C. G.; Stamatatos, T. C.; Papatriantafyllopoulou, C.; Tasiopoulos, A. J.; Wernsdorfer, W.; Perlepes, S. P.; Christou, G. *Inorg. Chem.* **2009**, *48*, 9737. (e) Yamaguchi, T.; Costes, J.-P.; Kishima, Y.; Kojima, M.; Sunatsuki, Y.; Bréfuel, N.; Tuchagues, J.-P.; Vendier, L.; Wernsdorfer, W. *Inorg. Chem.* **2010**, *49*, 9125. (f) Pasatoiu, T. D.; Etienne, M.; Madalan, A. M.; Andruh, M.; Sessoli, R. *Dalton Trans.* **2010**, *39*, 4802. (g) Gao, Y.; Zhao, L.; Xu, X.; Xu, G.-F.; Guo, Y.-N.; Tang, J.; Liu, Z. *Inorg. Chem.* **2011**, *50*, 1304. (h) Pasatoiu, T. D.; Sutter, J.-P.; Madalan, A. M.; Fellah, F. Z. C.; Duhayon, C.; Andruh, M. *Inorg. Chem.* **2011**, *50*, 5890. (i) Colacio, E.; Ruiz-Sanchez, J.; White, F. J.; Brechin, E. K. *Inorg. Chem.* **2011**, *50*, 7268.

(9) Novitchi, G.; Wernsdorfer, W.; Chibotaru, L. F.; Costes, J.-P.; Anson, C. E.; Powell, A. K. *Angew. Chem., Int. Ed.* **2009**, *48*, 1614.

(10) (a) Costes, J.-P.; Dahan, F.; Dupuis, A.; Laurent, J.-P. *Chem.—Eur. J.* **1998**, *4*, 1616. (b) Xu, Z.; Read, P. W.; Hibbs, D. E.; Hursthouse, M. B.; Malik, K. M. A.; Patrick, B. O.; Rettig, S. J.; Seid, M.; Summers, D. A.; Pink, M.; Thompson, R. C.; Orvig, C. *Inorg. Chem.* **2000**, *39*, 508. (c) Zhang, J.-J.; Hu, S.-M.; Zheng, L.-M.; Wu, X.-T.; Fu, Z.-Y.; Dai, J.-C.; Du, W.-X.; Zhang, H.-H.; Sun, R.-Q. *Chem.—Eur. J.* **2002**, *8*, 5742. (d) Bayly, S. R.; Xu, Z.; Patrick, B. O.; Rettig, S. J.; Pink, M.; Thompson, R. C.; Orvig, C. *Inorg. Chem.* **2003**, *42*, 1576. (e) Mori, F.; Ishida, T.; Nogami., T. *Polyhedron* **2005**, *24*, 2588. (f) Madalan, A. M.; Bernot, K.; Pointillart, F.; Andruh, M.; Caneschi, A. *Eur. J. Inorg. Chem.* **2007**, 5533. (g) Shiga, T.; Ito, N.; Hidaka, A.; Ōkawa, H.; Kitagawa, S.; Ohba, M. *Inorg. Chem.* **2007**, *46*, 3492. (h) Kong, X.-J.; Ren, Y.-P.; Long, L.-S.; Zheng, Z.; Nichol, G.; Huang, R.-B.; Zheng, L.-S. *Inorg. Chem.* **2008**, *47*, 2728. (i) Yamaguchi, T.; Sunatsuki, Y.; Ishida, H.; Kojima, M.; Akashi, H.; Re, N.; Matsumoto, N.; Pochaba, A.; Mroziński, J. *Inorg. Chem.* **2008**, *47*, 5736. (j) Costes, J.-P.; Yamaguchi, T.; Kojima, M.; Vendier, L. *Inorg. Chem.* **2009**, *48*, 5555. (k) Igarashi, S.; Kawaguchi, S.-i.; Yukawa, Y.; Tuna, F.; Winpenny, R. E. P. *Dalton Trans.* **2009**, 3140. (l) Papatriantafyllopoulou, C.; Stamatatos, T. C.; Efthymiou, C. G.; Cunha-Silva, L.; Paz, F. A. A.; Perlepes, S. P.; Christou, G. *Inorg. Chem.* **2010**, *49*, 9743.

(11) Pooransingh, N.; Pomerantseva, E.; Ebel, M.; Jantzen, S.; Rehder, D.; Polenova, T. *Inorg. Chem.* **2003**, *42*, 1256.

(12) Wernsdorfer, W. *Adv. Chem. Phys.* **2001**, *118*, 99.

(13) Sheldrick, G. M. *Acta Crystallogr., Sect. A* **2008**, *64*, 112.

(14) Kahn, O. *Molecular Magnetism*; VCH Publ. Inc.: New York, 1993.

(15) Cole, K. S.; Cole, R. H. *J. Chem. Phys.* **1941**, *9*, 341.